

A facile production of microporous carbon spheres and their electrochemical performance in EDLC

XiaoHong Xia, Lei Shi, HongBo Liu*, Li Yang, YueDe He

College of Materials Science and Engineering, Hunan University, Changsha, Hunan 410082, China

ARTICLE INFO

Article history:

Received 2 September 2010

Received in revised form

4 October 2011

Accepted 20 October 2011

Available online 29 October 2011

Keywords:

A. Microporous materials

C. Differential scanning calorimetry (DSC)

D. Raman spectroscopy

E. Electrochemical properties

ABSTRACT

In the absence of activation process, we prepared a series of carbon particles from saccharine, in which hydrothermal carbonization method was used. These particles have spherical or near-spherical morphology, controllable monodisperse particle size from the analyses of SEM. Raman and XRD results show that they are nongraphitizable. The BET surface area of these carbon spherules is around 400–500 m² g⁻¹ and the microporosity is about 84%, suggesting that the carbon particles are rich in micropores. The electrochemical behaviors were characterized by means of galvanostatic charging/discharging, cycle voltammetry and impedance spectroscopy. The results show that the specific capacitance of sucrose-based carbon spherule reached 164 F g⁻¹ in 30% KOH electrolyte and a high volumetric capacitance over 170 F cm⁻³ was obtained. These carbon spherules could be promising materials for EDLC according to their facile preparation way, low cost and high packing density.

© 2011 Elsevier Ltd. All rights reserved.

1. Introduction

Electric double-layer capacitors (EDLCs) are unique electrical storage devices exhibiting high power density (over 10 kW kg⁻¹) and long durability (over 10⁶ cycles), which allowed their applications for various power and energy requirements, e.g. backup power sources for electronic devices, engine start or acceleration for hybrid electric vehicles and electricity storage generated from solar or wind energy [1–3].

Many kinds of carbons with high specific surface areas and suitable pore structures have displayed great potential as active materials for EDLC [4–7]. Among various carbon materials, carbon with spherical morphology and nanopores has been proved practically to be competent for EDLC owing to its high packing density, low surface-to-volume ratio and maximal structural stability, etc.

Different methods have been used to synthesize carbon spheres [5,8,9]. Lee et al. have made microporous carbon nanospheres from an aromatic resin isotropic pitch through the precipitation [8]; Li et al. have prepared mesoporous carbon spheres by a polymerization-induced colloid aggregation method [5]. Ordered nanoporous carbon spheres have been synthesized through the inverse replication of the highly ordered MCM-41-type mesoporous silica template [9]. Among these methods, however, the surface area of the carbon sphere is quite

low [8] or the procedures are more complicated [5,9]. Compared to these methods, hydrothermal carbonization [10,11] is one of the most efficient way to produce carbon spheres and the procedure is rather simple.

Hydrothermal treatment of saccharine was firstly applied during the first half of the twentieth century to obtain information about the mechanism of natural coalification [8], by which a carbon-rich solid product could be obtained by a thermal treatment of water mixed with organic substances such as saccharine or simple compounds such as furfural at temperatures in the 150–350 °C range. However, not until recently, this process has generated widespread interest [10,11].

In our present work, several kinds of saccharine, such as β-cyclodextrin, sucrose and glucose were employed for fabricating carbon spherules by hydrothermal carbonization without activation. The electrochemical performance in EDLC of carbon spherules produced from those saccharine was firstly investigated in a 30 wt% KOH aqueous solution.

2. Experimental

2.1. Preparation of carbon samples

The preparation of carbon samples was carried out according to the following procedure: 80 mL saccharine solution of 8.4 mol L⁻¹ (calculated by carbon atom) was filled into a stainless steel autoclave, heated up to a temperature at 180 °C for 24 h. The resulting dark brown powder was washed by distilled water and

* Corresponding author. Tel.: +86 18684656260; fax: +86 073188823554.
E-mail address: xia_spring@163.com (H. Liu).

dried at 100 °C for 12 h. Then the powder was further pyrolyzed in a tube furnace in an argon atmosphere at 900 °C at 5 °C min⁻¹ and maintained the temperature for 1.5 h. Finally the black carbon powder was washed with distilled water and collected after drying at 120 °C for 12 h. The samples obtained from β -cyclodextrin, sucrose and glucose are denoted by HS-cd, HS-s and HS-g, and the carbon samples denoted by CS-cd, CS-s and CS-g, respectively.

2.2. Characterization of the carbon spherules

The morphology of the sample was investigated by a scanning electron microscope (JSM-6700F, JEOL, Japan). The structure of the sample was characterized by Raman spectra (laser confocal Raman spectrometer LABRAM-010, JY Company, France) and X-ray diffraction (Rigaku B/max-2400 X-ray diffractometer, Rigaku, Japan). Nitrogen adsorption and desorption isotherms of carbons were obtained at 77 K with an automatic adsorption apparatus (ASAP 2020, Micromeritics, USA). The BET SSA (S_{BET}) and total pore volumes (V_{tot}) were calculated using the Brunauer–Emmett–Teller equation and the single point method, respectively. The average pore diameter (D) was estimated from the equation $4V_{\text{tot}}/S_{\text{BET}}$. Micropore SSA (S_{mic}) was calculated by the t-plot method. The corresponding pore size distributions were calculated with the desorption data based on the BJH method.

2.3. Electrochemical measurements of the carbon spherules

Carbon samples (active material), carbon black (conductivity enhancing material) and PTFE (60 wt% solution, binder) were mixed in a mass ratio of 90:5:5 and dispersed in deionized water (the mass ratio of carbon to water was set as 1:2). After homogenization in a mortar, the slurry was rolled into a thin film of uniform thickness (0.5 ± 0.1 mm). From this film, 12 mm circular electrodes were punched out and pressed onto nickel foam (as a current collector). The carbon coated nickel foam was then immersed in a 30% (wt%) KOH solution under vacuum for ca. 3 h before testing.

Electrochemical measurements (CV, EIS) were performed on an electrochemical workstation CHI660A (Chenhua Instrument Corp., China) at room temperature, using two-electrode electrochemical capacitor cells. Cyclic voltammograms were recorded from 0 to 1 V at various sweep rates and the Nyquist plots were recorded potentiostatically (0 V) by applying an alternating voltage of 5 mV amplitude in the 100 kHz–1 MHz frequency range. The constant-current discharge–charge tests were conducted in the voltage range of 0–1 V with a Battery Tester (Land, Wuhan, China) at different specific current.

3. Results and discussion

Fig. 1 shows SEM images of the products of β -cyclodextrin, sucrose and glucose after hydrothermal treatment (Fig. 1a, c and e) and carbonization (Fig. 1b, d and f). As shown in Fig. 1, after hydrothermal treatment at 180 °C microspheres with smooth surface in a diameter of 0.5–1.5 μm range were obtained in three samples. Mild shrinkage was detected after carbonization due to the elimination of noncarbon atoms at high temperature and the aggregation phenomenon was more obvious in glucose sample. The aggregated CS-g particles are close to spheric in morphology, albeit lacking a clear boundary around a particle. In our previous work, hydrothermal reactions occurred in glucose and sucrose solution at 150 °C, whereas no change was detected in β -cyclodextrin until the temperature was increased up to 180 °C. These phenomena disclose that the larger the saccharide molecule is, the higher the temperature is needed for the onset of

hydrothermal reaction, since β -cyclodextrin has the largest molecular weight among the three saccharide when other reaction conditions are totally same. The resistance of β -cyclodextrin to decomposition may be a consequence of the fact that the hydroxyl groups of the glucose residues present in the structure of the β -cyclodextrin form hydrogen bonds that hold the polymeric chains firmly together and side-by-side [12].

The structure of carbon samples was characterized by Raman spectra and XRD. From the Raman spectra (Fig. 2), the carbonized samples exhibit two broad overlapping bands at around 1320 cm⁻¹ (D-mode) and 1592 cm⁻¹ (G-mode). The D and G bands are usually assigned to the bands of disordered carbon and graphitized carbon, respectively. The relative intensity ($I_{\text{D}}/I_{\text{G}}$) has been used to determine the graphitization degree of carbon species. The $I_{\text{D}}/I_{\text{G}}$ of CS-cd, CS-s and CS-g was estimated to be about 1.05, 1.15 and 1.12, respectively, which reveal the presence of C sp² atoms in benzene or condensed benzene rings of amorphous (partially hydrogenated) carbon [13,14]. The XRD pattern was shown in Fig. 3. The diffraction profile of all carbon samples show two diffraction peaks at the diffraction angle of carbon (002), a broad peak around 24.8° and a sharp peak at 26.5°, which indicates there are two different carbon structures in them [15]. Broad peak around 43.0° 2θ has been observed and this may be assigned to the (10) (overlapped 100 and 101) diffraction of disordered stacking of micrographites [16], confirming the Raman pattern in Fig. 2. During the course of hydrothermal treatment, saccharine molecules undergo a series of resetting reactions including intermolecular dehydration and aldol condensation, and then the aromatization of polymers takes place. A relative good graphitic net plane would be formed after carbonization. However, since the transition time from fluid phase to solid phase is not long that the thickness of the graphitic plane would be small.

Their nitrogen adsorption–desorption isotherms are shown in Fig. 4a. The isotherms of the three samples correspond to type I nitrogen adsorption–desorption isotherm according to the IUPAC classification, which means there are mainly micropores. Sharp slopes were illustrated in the isotherms of CS-g and CS-cd over relative pressure 0.8, indicating besides micropores they have macropores [17]. Fig. 4b shows the BJH pore size distributions of these carbon spherules. It is clear that all three carbon samples exhibit predominantly micropores and meso- and macropores about 30–60 nm were displayed in CS-g and CS-cd samples, which is in good agreement with Fig. 4a. A majority of pore volume was associated with pores ranging from pore diameter of 2–5 nm. Detailed characteristics of the pore structure of all samples are collected in Table 1. The results show that CS-s illustrates a maximum BET surface area of 510 m² g⁻¹ and total pore volume of 0.25 cm³ g⁻¹.

The electrode pairs from the three carbon samples were tested in 30% KOH aqueous solution at room temperature. The charge/discharge curves of carbon samples between the voltage range of 0.01–1 V at 1 mA cm⁻² are displayed in Fig. 5 and the specific capacitances at different discharge density were studied as shown in Table 2. The charge/discharge behavior of the carbon samples in 30 wt% KOH solution is highly reversible. The discharge curves are approximately linear and symmetric to their corresponding charge curves. At the beginning of the discharge, no sharp change in voltage is observed. That is, the equivalent series resistance (ESR) of the EDLCs is rather low. As seen in Table 2, the capacitance decrease with discharge current, which is mainly because the potential difference between the mouth and the bottom of the micropores increases with the current due to ohmic resistance of the electrolyte in the axial direction of micropores [18]. At high current density, electrolyte ions cannot move fast enough to the bottom of the micropores, so the capacitance declined. The maximum specific capacitance value was achieved

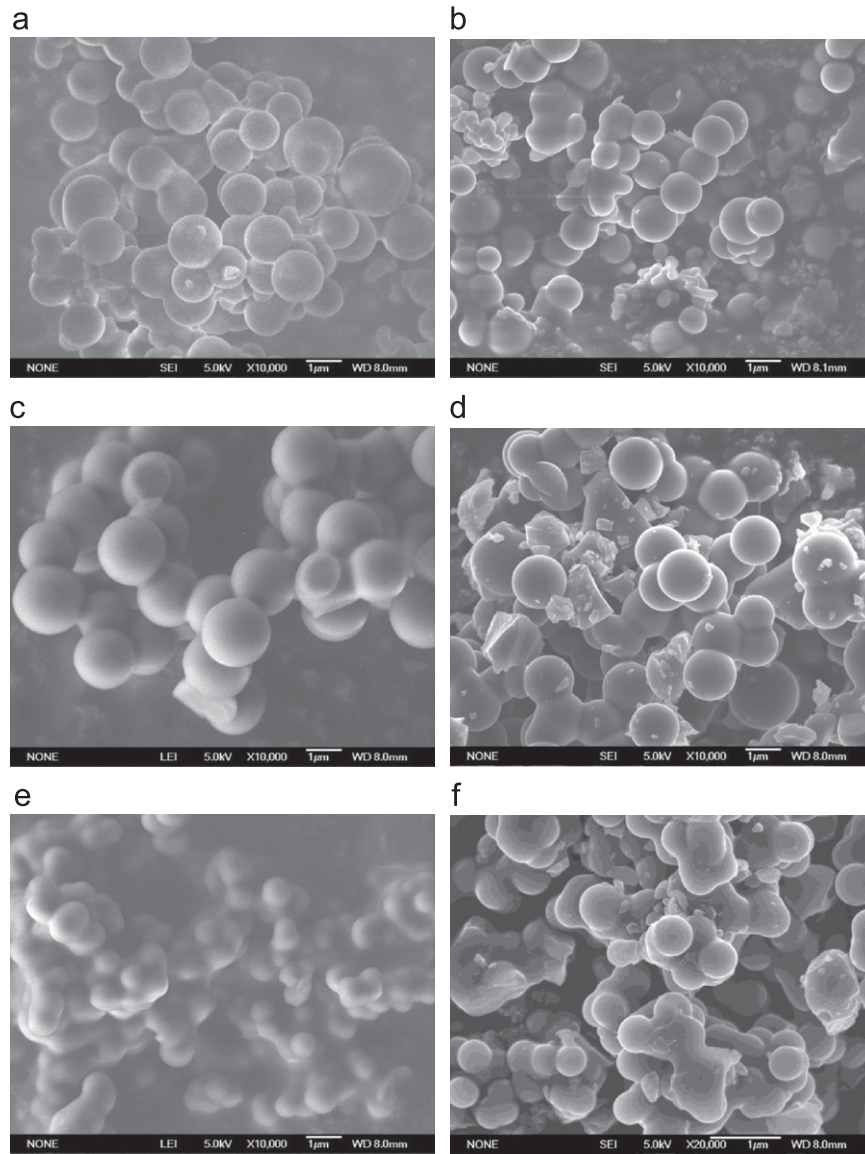


Fig. 1. SEM images of the (a) HS-cd, (c) HS-s, (e) HS-g and (b) CS-cd, (d) CS-s, (f) CS-g.

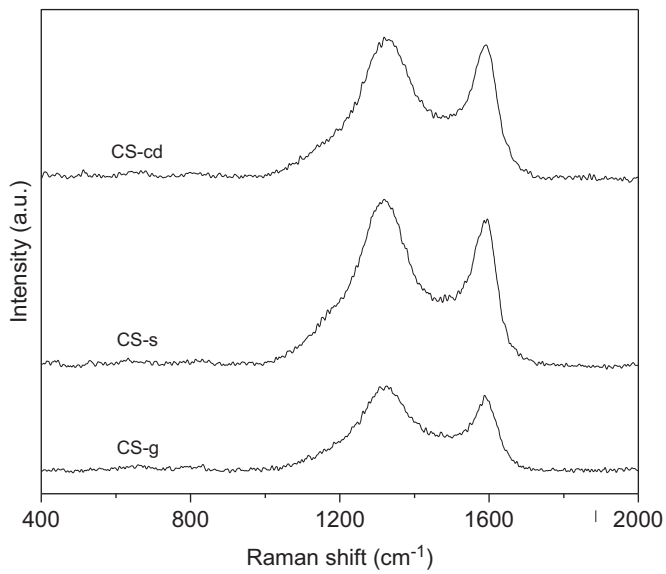


Fig. 2. The Raman spectra of the carbon spherule samples.

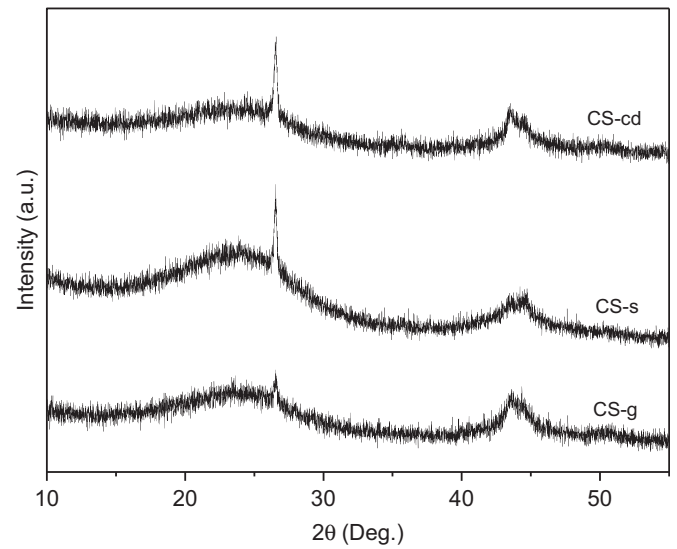


Fig. 3. The XRD patterns of the carbon spherule samples.

with the sample of CS-s and the area specific capacitance of CS-s is about $30 \mu\text{F cm}^{-2}$, which is higher than some other carbonaceous materials [19–21]. The high specific capacitance suggests that most of the micropore surface area in this carbon is accessible at low current loads (1 mA cm^{-2}) to electrolyte ions and double-layer formation. The reason may be that carbon samples prepared by polycondensation and carbonization of organic carbon precursor have more continuous micropores, like carbon aerogel [22], so the accessibility of micropores was enhanced and more efficient charge storage in EDLC was achieved. However, pores in activated carbons were primarily formed by the etching process from surface to inside of activating

agent and the pore structure was not continuous porosity. So the area specific capacitance is relatively low [21].

Fig. 6 shows cyclic voltammograms at the 2 mV s^{-1} sweep rate obtained for the capacitors using CS-cd, CS-s and CS-g as electrodes, respectively. At the identical scan rate, the most ideal capacitive behavior was observed for CS-s with a steepest current change at the switching potential (0 and 1.0 V), resulting in a most rectangular-shaped $I-V$ curve. The faster change at the switching potentials in the cyclic voltammogram of CS-s than CS-cd and CS-g stems from the faster re-organization of the double layer in CS-s, probably owing to faster ionic motions in its micropores. In addition, higher capacitance was obtained from CS-s than CS-cd and CS-g (173 F g^{-1} , 156 F g^{-1} and 166 F g^{-1} , respectively), suggesting that more surface area of the carbon was accessed by the electrolyte ions due to the higher specific area and more

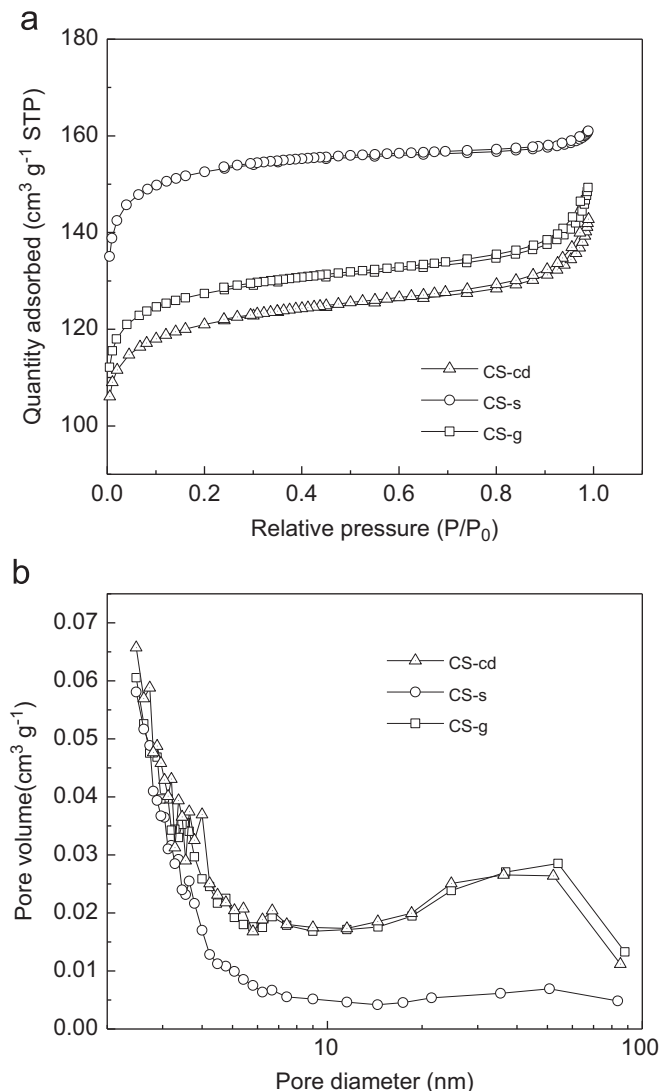


Fig. 4. Nitrogen sorption isotherms (a) and pore size distribution (b) of the carbon spherule samples.

Table 1
The specific surface area and pore structures of carbon spherules.

Samples	BET surface area ($\text{m}^2 \text{ g}^{-1}$)	Microsurface area ($\text{m}^2 \text{ g}^{-1}$)	Pore volume ($\text{cm}^3 \text{ g}^{-1}$)	Micropore volume ($\text{cm}^3 \text{ g}^{-1}$)	Microporosity (%)	Average pore diameter (nm)
CS-cd	405.8	334.7	0.22	0.17	82.7	2.14
CS-s	510.6	433.4	0.25	0.21	84.9	1.94
CS-g	426.9	359.7	0.23	0.17	84.3	2.13

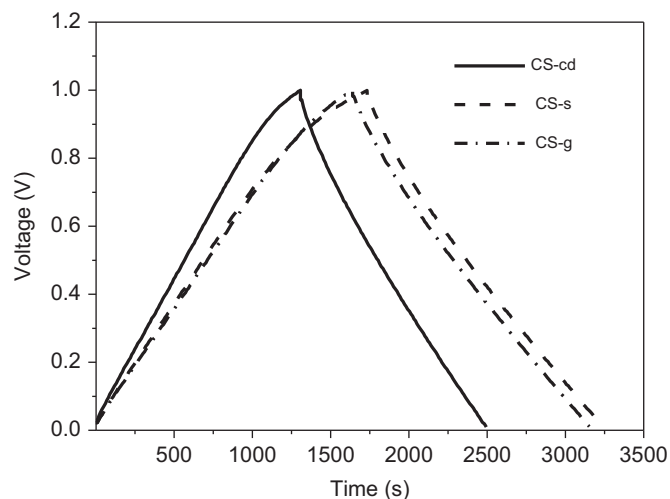


Fig. 5. The charge/discharge curves of carbon spherules between the voltage range of 0.01–1 V at 1 mA cm^{-2} .

Table 2
The specific capacitances at the CS-s electrodes for electrolyte in 30% KOH aqueous electrolyte.

Current density (mA cm^{-2})	Specific capacitance of carbon spherules					
	CS-cd		CS-s		CS-g	
	$\text{F g}^{-1 \text{ a}}$	$\text{F cm}^{-3 \text{ b}}$	$\text{F g}^{-1 \text{ a}}$	$\text{F cm}^{-3 \text{ b}}$	$\text{F g}^{-1 \text{ a}}$	$\text{F cm}^{-3 \text{ b}}$
1	145	147	164	170	162	173
3	125	127	154	159	151	161
5	115	116	148	153	142	152
8	105	106	144	148	137	146
10	102	103	143	147	132	141
15	93	94	138	143	127	135
20	92	93	134	138	116	124

^a Referred to the carbon mass in a single electrode.

^b Referred to the electrode volume.

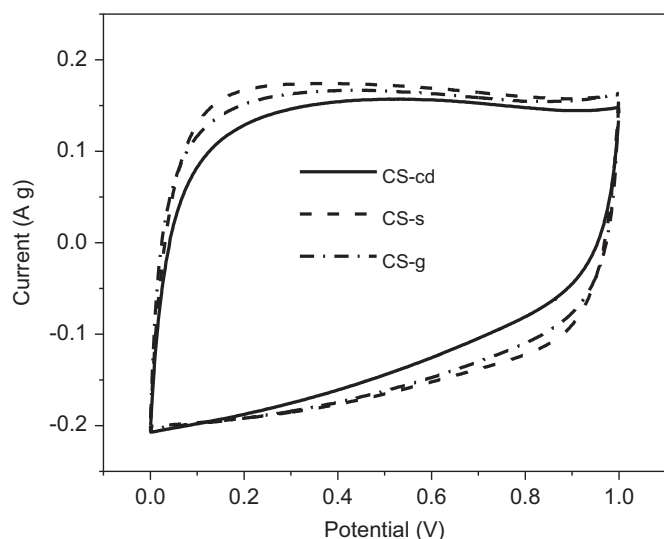


Fig. 6. Cyclic voltammograms at the 5 mV s^{-1} sweep rate using CS-cd, CS-s and CS-g as electrodes, respectively.

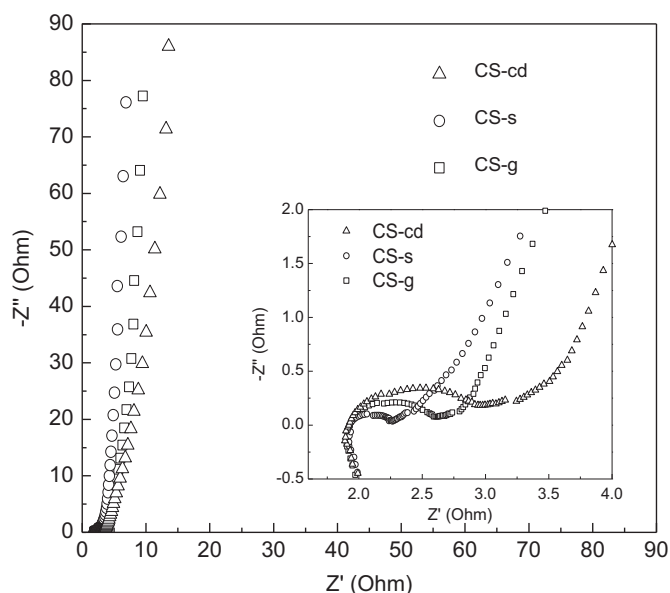


Fig. 7. Nyquist plots using CS-cd, CS-s and CS-g as electrodes.

reasonable pore distribution of CS-s, which is in agreement with the result obtained from the galvanostatic study. (See Table 2).

Fig. 7 shows typical Nyquist plots in a frequency range of 100 kHz–1 mHz for the capacitors with the three carbon spherules. In the high frequency region, a depressed semicircle occurred, indicating a parallel combination of resistive and capacitive components. Electrolyte resistance can be estimated from the crossover point of the highest frequency with the real part of impedance. The high frequency loop is linked to the accessible electrode porosity to the electrolyte. The loop diameter can be considered as the resistance from the mass transport (i.e., transport of electrolyte ions within micropores of porous carbon), and termed charge transport resistance. CS-s has less semicircle than other samples (the inset in Fig. 7), which indicates smaller charge transfer resistance.

Several electrical circuits were estimated by nonlinear least squares fitting of the experimental impedance data. The equivalent circuit shown in Fig. 8 was found to obtain excellent fits down to frequencies including the low-frequency vertical line, in which R_s is the bulk solution resistance, C_c the contact

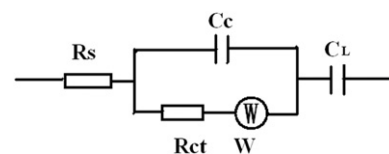


Fig. 8. Equivalent circuit for the impedance spectra of the carbon electrodes.

Table 3

Simulation results of equivalent circuit elements from the simulation of the impedance data.

Electrode samples	R_s (Ω)	C_c (μF)	R_{ct} (Ω)	C_L (F g^{-1})	χ^2
CS-cd	2.8	469.1	0.939	147.3	3.54×10^{-3}
CS-s	2.5	1068.0	0.265	173.4	5.79×10^{-3}
CS-g	2.1	637.2	0.504	161.4	8.97×10^{-3}

Table 4

The error of equivalent circuit elements from the simulation of the impedance data.

Electrode samples	Error (%)			
	R_s	W	R_{ct}	C_L
CS-cd	1.164	4.643	5.299	2.512
CS-s	1.473	7.24	18.94	2.923
CS-g	1.905	7.539	11.24	3.698

capacitance, R_{ct} the contact resistance, and a Warburg diffusion element (Δ) attributable to the diffusion of ions. Besides, the capacitive nature of the carbon-based electrode in the low-frequency domain could be reasonably presented as a low-frequency capacitance, C_L . The simulation results of the impedance data for different carbon electrodes using ZSimpWin software and the errors of the parameters for corresponding equivalent circuits from fitting EIS data are illustrated in Tables 3 and 4, respectively.

The average error (χ^2) of the fits in Table 3 for the different impedance spectra of the carbon electrode is relatively small, ranging from 3.54×10^{-3} to 8.97×10^{-3} while the error of the corresponding element is in the range of 1.164–18.94% (shown in Table 4), which prove that the selected equivalent circuits are proper for the investigated electrodes. From a comparison of R_{ct} and C_L of different carbon electrodes in Table 3, the ionic charge transfer resistance of CS-s is the smallest while its C_L is the biggest among the carbon electrodes. That is to say, the CS-s electrode has the fastest charge transfer within micropores and the biggest capacitance, which is in good agreement with the results from the cyclic voltammetric measurements and galvanostatic study.

4. Conclusion

Hydrothermal carbonization method without activation was adopted to prepare nanoporous carbon microspheres, using β -cyclodextrin, sucrose and glucose as carbon precursors. The method was proved to be an effective process to produce carbon spherules with specific surface area ($400\text{--}500 \text{ m}^2 \text{ g}^{-1}$) and a porosity accessible to electrolyte ions (average micropore sizes around 1.9–2.1 nm). The electrochemical tests for these carbon spherules were performed in 30 wt% KOH aqueous electrolyte. Among these samples, CS-s exhibits an ideal electric capacity of 164 F g^{-1} at 1 mA cm^{-2} and good capacitance maintenance of 82% even at 20 mA cm^{-2} . A higher volumetric capacitance of 170 F cm^{-3} was

achieved due to more available surface area and high packing density of the carbon spherule. This enhances the industrial potential of the carbon spheres for small electric power sources.

Acknowledgment

Financial support by the National Natural Science Foundation of China (no. 50872032) and the Fundamental Research Funds for the Central Universities (no.531107040185).

References

- [1] B.E. Conway, *Electrochemical Supercapacitors: Scientific Fundamentals and Technological Applications*, Kluwer Academic/Plenum Publishers, New York, 1999.
- [2] J. Chmiola, G. Yushin, Y. Gogotsi, et al., *Science* 313 (2006) 1760–1763.
- [3] A.S. Arico, P. Bruce, B. Scrosati, et al., *Nat. Mater.* 4 (2005) 366–377.
- [4] D.W. Wang, F. Li, M. Liu, et al., *Angew. Chem. Int. Ed.* 47 (2008) 373–376.
- [5] W. Li, D. Chen, Z. Li, et al., *Electrochem. Commun.* 9 (2007) 569–573.
- [6] Ch.X. Zhang, D.H. Long, B.L. Xing, et al., *Electrochem. Commun.* 10 (2008) 1809–1811.
- [7] M.S. Balathanigaimani, W.G. Shima, M.J. Lee, et al., *Electrochem. Commun.* 10 (2008) 868–871.
- [8] S.I. Lee, S. Mitani, Ch.W. Park, et al., *J. Power Sour.* 139 (2005) 379–383.
- [9] T. Nakamura, Y. Yamada, K. Yano, *Microporous Mesoporous Mater.* 117 (2009) 478–485.
- [10] Q. Wang, H. Li, L. Chen, et al., *Solid State Ionics* 152–153 (2002) 43–50.
- [11] M. Sevilla, A.B. Fuertes, *Carbon* 47 (2009) 2281–2289.
- [12] Sh. Saka, T. Ueno, *Cellulose* 6 (1999) 177–191.
- [13] A.C. Ferrari, J. Robertson, *Phys. Rev. B* 61 (2000) 14095–14107.
- [14] J. Schwan, S. Ulrico, V. Batori, H. Ehrhardt, *J. Appl. Phys.* 80 (1996) 440–447.
- [15] R. Xue, H. Liu, P.P. Wang, Z. Shen, *Carbon* 47 (2008) 318–320.
- [16] Q. Wang, X.Y. Liang, W.M. Qiao, et al., *Fuel Process. Technol.* 90 (2009) 381–387.
- [17] J.S. Ima, S.J. Parkb, Y.S. Lee, *J. Colloid Interface Sci.* 314 (2007) 32–37.
- [18] Ch.T. Hsieh, H. Teng, *Carbon* 40 (2002) 667–674.
- [19] M. Olivares-Marín, J.A. Fernández, M.J. Lázaro, *Mater. Chem. Phys.* 114 (2009) 323–327.
- [20] A. Bagreev, J.A. Menendez, I. Dukhno, Y. Tarasenko, T.J. Bandoz, *Carbon* 42 (2004) 469–476.
- [21] K. Jurewicz, R. Pietrzakb, P. Nowicki, H. Wachowska, *Electrochim. Acta.* 53 (2006) 5469–5475.
- [22] S.W. Hwang, S.H. Hyun, *J. Non-Cryst. Solids* 347 (2004) 238–245.